A comparison of 4 advection schemes for use in unstructured grid ocean modelling

E. Hanert[1,2], D.Y. Le Roux[3], V. Legat[2], E. Deleersnijder[1]
[1]Université Catholique de Louvain, Institut d'Astronomie et de Géophysique G. Lemaître,
2 Chemin du Cyclotron, 1348 Louvain-la-Neuve, Belgium
[2]Université Catholique de Louvain, Centre for Systems Engineering and Applied Mechanics,
4 Avenue Georges Lemaître, 1348 Louvain-la-Neuve, Belgium
[3]Université Laval, Département de Mathématiques et de Statistique,
Québec, QC, G1K 7P4, Canada
email: hanert@astr.ucl.ac.be, dleroux@mat.ulaval.ca, vl@mema.ucl.ac.be, ericd@astr.ucl.ac.be

Abstract— **We study advection schemes for unstructured grid ocean models. Four linear advection schemes are investigated by solving a scalar transport equation. Schemes under consideration include continuous, non-conforming and discontinuous finite elements and finite volumes. A comprehensive derivation of the numerical schemes is presented and dispersion and conservation properties are discussed. An assessment is made by performing the test problem introduced by Hecht et al. [J. Geophys. Res. 100 (1995) 20763-20778] in which a passive scalar field is advected through an analytical Stommel gyre. It is found that continuous finite elements and finite volumes have some difficulties to represent accurately solutions with steep gradients. As a result they are prone to generate unphysical oscillations. On the other hand, discontinuous and non-conforming finite element schemes perform better. This is due to their higher flexibility that makes them better suited to highly sheared flows.**

Keywords— **Ocean modelling, unstructured grids, advection schemes**

I. Introduction

OCEAN circulation strongly depends on water density gradients. Empirical parameterizations permit to express water density in terms of water temperature and salinity. These quantities are transported by the flow and diffused by eddy mixing. Their evolution is thus governed by an advection-diffusion equation. Since this equation is usually dominated by advection, it is especially important that numerical models accurately represent advective processes. This is however not straightforward, especially with Eulerian schemes.

The vast majority of ocean models use a structured grid and the finite difference method. This is mainly due to the inherent simplicity of structured grids. Nevertheless, in the last years much attention has been paid to unstructured grids (e.g. [1], [2], [3], [4], [5], [6]). Their ability to represent complex geometries and localized phenomena sounds attractive given the high complexity of oceanic flows.

In unstructured grid ocean modelling, the numerical treatment of advection is still a central issue. The choice of a convenient numerical method has not been thoroughly discussed yet and many advection schemes commonly used in engineering seem to be ignored by ocean modellers. A convenient scheme should involve a compromise between quality and computational cost. The quality of the solution must be assessed in the context of ocean modelling.

In the present paper, we evaluate four linear advection schemes applied to two-dimensional tracer transport within a Stommel gyre. This test problem is relevant in ocean modelling where intense boundary flows with strong shear are often constraining for numerical methods. Herein we consider finite volumes and continuous, discontinuous and non-conforming finite elements. They are quite representative of available Eulerian methods for unstructured grids.

Among the four methods examined in the present paper, continuous finite elements are the most often used in unstructured grid ocean models. They may be stabilized with Galerkin least-squares [6] or pseudo residual-free bubble functions [5] to obtain better results. Finite volumes are well suited to solve conservative law problems. They are based on a decomposition of the computational domain into control volumes and on flux budgets between those volumes. More details may be found in [7]. Discontinuous finite elements were first analysed by [8]. They have been studied intensively in the last decade and applied to a large number of problems. A comprehensive review may be found in [9]. Non-conforming finite elements have been introduced by [10] to solve Stokes equations. They have proved to be well suited to represent shallow water oceanic flows ([11], [12]).

II. Continuous problem

We consider the following advection-diffusion problem: Let Ω be an open bounded domain in $\mathbf{R}^n$ $(n = 2, 3)$, we seek the scalar function $s(\mathbf{x}, t)$ which is the solution of the following boundary value problem:

$$\frac{\partial s}{\partial t} + \boldsymbol{\nabla} \cdot (\mathbf{u}s) = \boldsymbol{\nabla} \cdot (K \boldsymbol{\nabla} s) \qquad \text{on } \Omega, \forall t, \quad (1)$$

$$K \boldsymbol{\nabla} s \cdot \mathbf{n} = \mathbf{0} \qquad \text{on } \partial\Omega, \quad (2)$$

$$s(\mathbf{x}, 0) = s_0(\mathbf{x}) \qquad \text{on } \Omega, \quad (3)$$

where $\partial\Omega \subset \mathbf{R}^{n-1}$ is the domain boundary, $\mathbf{u} = \mathbf{u}(\mathbf{x})$ is a given divergence-free velocity field such that $\mathbf{u} \cdot \mathbf{n} = \mathbf{0}$ on $\partial\Omega$, $\mathbf{n}$ is the unit normal vector pointing out of the domain Ω and K is a constant diffusion coefficient.

III. Domain partitions

Let $\mathcal{P}$ be a partition of the domain Ω into N_Ω disjoint open subdomains Ω_i:

$$\bar{\Omega} = \bigcup_{i=1}^{N_\Omega} \bar{\Omega}_i \quad \text{and} \quad \Omega_i \cap \Omega_j = \emptyset \quad \text{for } i \neq j.$$

Each subdomain Ω_i has a boundary $\partial\Omega_i$. Let Γ be the ensemble of interelement boundaries $\Gamma_l = \partial\Omega_i \cap \partial\Omega_j$ with

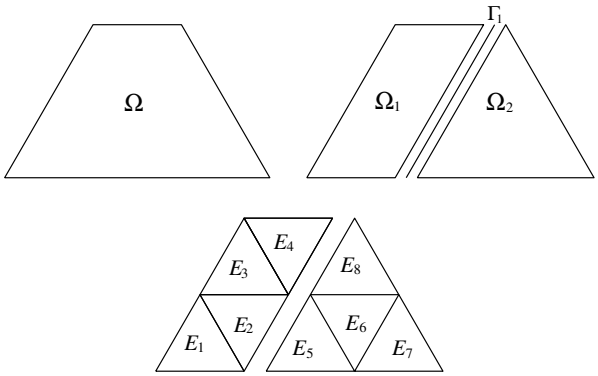

Fig. 1. Example of partition of the domain Ω into two subdomains Ω_1 and Ω_2. The segment between Ω_1 and Ω_2 is denoted Γ_1. Each subdomain is partitioned into triangles E_e $(1 \leq e \leq 8)$. For the present example, $N_\Omega = 2$, $N_\Gamma = 1$, $N_E = 8$, $N_V = 9$ and $N_S = 16$.

$i > j$ inside the domain, with all possible combinations:

$$\bar{\Gamma} = \bigcup_{l=1}^{N_\Gamma} \bar{\Gamma}_l \quad \text{and} \quad \Gamma_l \cap \Gamma_m = \emptyset \quad \text{for } l \neq m,$$

where N_Γ is the number of element in Γ. With each $\Gamma_l \in \Gamma$ we associate a unique unit normal vector $\mathbf{n}$ which points from Ω_i to Ω_j. We also build a triangulation of Ω such that each element E_e belongs to only one subdomain Ω_i. Hence the domain Ω is such that:

$$\bar{\Omega} = \bigcup_{e=1}^{N_E} \bar{E}_e \quad \text{and} \quad E_e \cap E_f = \emptyset \quad \text{for } e \neq f,$$

where N_E is the number of triangles in Ω. The total number of vertices and segments in the triangulation are denoted N_V and N_S. An illustration of the different partitions is given in Fig. 1.

In the present paper we also consider a finite volume scheme and thus introduce a partition of the computational domain Ω into disjoint open control volumes V_n:

$$\bar{\Omega} = \bigcup_{n=1}^{N_V} \bar{V}_n \quad \text{and} \quad V_n \cap V_p = \emptyset \quad \text{for } n \neq p.$$

Control volumes are built by joining the barycenter of each triangle E_e to the centres of the three faces (Fig. 2). Such a partition of Ω corresponds to the Voronoï diagram of the triangulation if the latter is a Delaunay triangulation.

IV. A non-continuous variational or weak formulation

We now proceed with the derivation of a non-continuous weak formulation of problem (1) on a partitioned domain Ω. First of all we multiply (1) with a test function $\hat{s}$ belonging to a function space $\mathcal{S} = \{v \in L^2(\Omega) : v_{|\Omega_i} \in H^1(\Omega_i),\ \forall \Omega_i \in \mathcal{P}\}$. The equation is then integrated by parts on the partition $\mathcal{P}$ of Ω:

$$\sum_{i=1}^{N_\Omega} \int_{\Omega_i} \Big(\frac{\partial s}{\partial t}\hat{s} - s\mathbf{u}\cdot\boldsymbol{\nabla}\hat{s} + K\boldsymbol{\nabla}s\cdot\boldsymbol{\nabla}\hat{s} \Big)\, \mathrm{d}\Omega$$

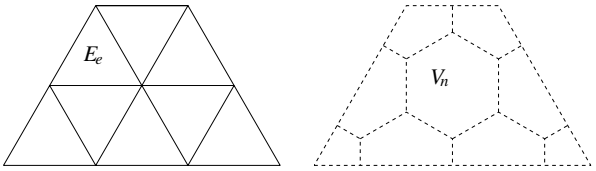

Fig. 2. Partitions of Ω into triangles (left) and the corresponding control volumes partition (right). The control volumes (dashed lines) are built by joining the barycenter of each triangle to the center of the three faces.

$$+ \sum_{l=1}^{N_\Gamma} \int_{\Gamma_l} \Big\{ \langle s\mathbf{u}\cdot\mathbf{n}\rangle [\hat{s}] + [s\mathbf{u}\cdot\mathbf{n}] \langle \hat{s} \rangle \Big\}\, \mathrm{d}\Gamma$$

$$- \sum_{l=1}^{N_\Gamma} \int_{\Gamma_l} \Big\{ \langle K\boldsymbol{\nabla}s\cdot\mathbf{n}\rangle [\hat{s}] + [K\boldsymbol{\nabla}s\cdot\mathbf{n}] \langle \hat{s} \rangle \Big\}\, \mathrm{d}\Gamma = 0, \quad (4)$$

where $[f] = f_{|\Omega_i} - f_{|\Omega_j}$ and $\langle f \rangle = \frac{1}{2}(f_{|\Omega_i} + f_{|\Omega_j})$ respectively denote the jump and average of f on an interior edge Γ_l. The restriction of f on Ω_i is denoted $f_{|\Omega_i}$.

The weak formulation is obtained by adding weak continuity constraints to equation (4). This is due to the elliptic nature of the problem which requires the continuity of the solution values and diffusive fluxes between subdomains. Hence, the weak formulation reads: Find $s(\mathbf{x}, t) \in \mathcal{S}$ such that

$$\sum_{i=1}^{N_\Omega} \int_{\Omega_i} \Big(\frac{\partial s}{\partial t}\hat{s} - s\mathbf{u}\cdot\boldsymbol{\nabla}\hat{\mathbf{s}} + K\boldsymbol{\nabla}s\cdot\boldsymbol{\nabla}\hat{s} \Big)\, \mathrm{d}\Omega$$

$$+ \sum_{l=1}^{N_\Gamma} \int_{\Gamma_l} \Big\{ \langle s\mathbf{u}\cdot\mathbf{n}\rangle [\hat{s}] + [s\mathbf{u}\cdot\mathbf{n}] \langle \hat{s} \rangle \Big\}\, \mathrm{d}\Gamma$$

$$- \sum_{l=1}^{N_\Gamma} \int_{\Gamma_l} \Big\{ \langle K\boldsymbol{\nabla}s\cdot\mathbf{n}\rangle [\hat{s}] + [K\boldsymbol{\nabla}s\cdot\mathbf{n}] \langle \hat{s} \rangle \Big\}\, \mathrm{d}\Gamma$$

$$+ \sum_{l=1}^{N_\Gamma} \int_{\Gamma_l} \Big\{ [s][a(\hat{s})] + 2[K\boldsymbol{\nabla}s\cdot\mathbf{n}] \langle b(\hat{s}) \rangle \Big\}\, \mathrm{d}\Gamma = 0, \quad (5)$$

$\forall \hat{s} \in \mathcal{S}$. The functions $a(\hat{s})$ and $b(\hat{s})$ can be selected to weigh the importance of the continuity constraints versus the advection-diffusion equation. Let us emphasize that continuity constraints are only weakly satisfied by the solution of problem (5). The solution of the weak formulation that we derived is not continuous between subdomains. However, the solution of the strong formulation or classical weak formulation belongs to $H^1(\Omega)$. In such a formulation, strong enforcement of the continuity of the solution and weak continuity of the fluxes is automatically obtained, without the need to add penalty terms. Algebraic details, about the way equation (4) and problem (5) are derived, can be found in [18].

Elliptic problems require the continuity of the solution in all directions while purely hyperbolic problems only require continuity along characteristics. In order to meet those

demands, we consider the following expression for $a(\hat{s})$:

$$a(\hat{s}) = \begin{cases} \frac{K}{|\Gamma_l|}\hat{s} + \mathbf{u}\cdot\mathbf{n}(\lambda - 1/2)\hat{s} & \text{on } \Omega_i, \\ \frac{K}{|\Gamma_l|}\hat{s} + \mathbf{u}\cdot\mathbf{n}(\lambda + 1/2)\hat{s} & \text{on } \Omega_j, \end{cases}$$

where $|\Gamma_l|$ is the measure of Γ_l. The first term in the expression of $a(\hat{s})$ enforces the continuity of the solution in all directions [19]. It depends on the diffusion coefficient in order to increase the constraint as diffusion increases. The second term only demands the continuity of the solution values along characteristics. This amounts to impose the continuity of the advective fluxes. The latter constraint is the only one which remains when $K = 0$. The parameter $\lambda \in [-1/2, 1/2]$ permits to orient the advective flux. A centered advection scheme is obtained by choosing $\lambda = 0$. Such a scheme is not the best suited to strongly advective flows since it is directionally symmetric contrary to advection. As a result, it may easily generate false extrema. A more stable scheme can be derived by taking into account the directionally oriented nature of the flow and thus selecting $\lambda = \frac{1}{2}\text{sign}(\mathbf{u}(\mathbf{x})\cdot\mathbf{n}(\mathbf{x}))$. This can be interpreted as an upwind scheme that permits to avoid many unphysical ripples in the solution. This parametrization will be used from now on to discretize the advective flux. To discretize the diffusive fluxes, we assume that diffusion is an isotropic phenomenon. Hence the diffusive flux continuity constraint should not be oriented and we choose:

$$b(\hat{s}) = \hat{s}/2.$$

For a 3D oceanic flow, horizontal and vertical diffusivities are usually different and an other expression for $b(\hat{s})$ should then be selected. There are of course many possibilities for $a(\hat{s})$ and $b(\hat{s})$ which give different formulations.

Finally, the weak or variational formulation of the boundary value problem reads: Find $s(\mathbf{x}, \mathbf{t}) \in \mathcal{S}$ such that

$$\sum_{i=1}^{N_\Omega} \int_{\Omega_i} \left(\frac{\partial s}{\partial t}\hat{s} - s\mathbf{u}\cdot\boldsymbol{\nabla}\hat{s} + K\boldsymbol{\nabla}s\cdot\boldsymbol{\nabla}\hat{s} \right) \mathrm{d}\Omega \qquad (6)$$

$$+ \sum_{l=1}^{N_\Gamma} \int_{\Gamma_l} \left(\langle s\mathbf{u}\cdot\mathbf{n}\rangle_\lambda [\hat{s}] - \langle K\boldsymbol{\nabla}s\cdot\mathbf{n}\rangle [\hat{s}] + \tfrac{K}{|\Gamma_l|}[s][\hat{s}] \right) \mathrm{d}\Gamma = 0$$

$\forall \hat{s} \in \mathcal{S}$. The notation $\langle f \rangle_\lambda$ represents the weighed average of f on the segment Γ_l:

$$\langle f \rangle_\lambda = (1/2 + \lambda) f_{|\Omega_i} + (1/2 - \lambda) f_{|\Omega_j}.$$

The variational formulation (6) involves the computation of upwind advective fluxes and centered diffusive fluxes on the interfaces between subdomains. It also involves the computation of a weak continuity constraint term to prevent sharp discontinuities in the solution while solving elliptic problems.

V. Discrete equations

We now construct a approximation s^h to the exact solution of problem (1)-(2)-(3) in a finite dimensional space $\mathcal{S}^\langle \subset \mathcal{S}$:

$$s \approx s^h = \sum_{i=1}^{N} S_i \phi_i,$$

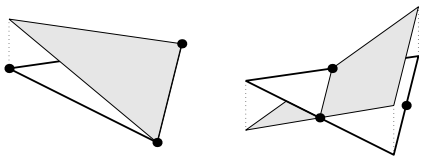

Fig. 3. Shape functions (in grey) associated with continuous and discontinuous approximations (left) and non-conforming approximations (right).

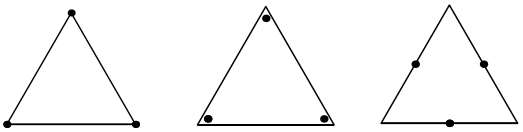

Fig. 4. Nodal values (•) distributions for the linear continuous (left), discontinuous (centre) and non-conforming (right) approximations.

where S_i and ϕ_i are the nodal value and the basis function associated with node i respectively. The number of nodal values is denoted N. In the present paper, we only consider consider continuous, discontinuous and non-conforming linear approximations. The shape functions used for those approximations are represented on Fig. 3. A shape function is always equal to one on the associated node and equal to zero on any other node. As seen in Fig. 4, the nodal values of the continuous approximation are lying on the vertices of the triangulation and thus belong to many elements. The discrete solution is therefore continuous between triangles. For the discontinuous approximation, the nodal values still lie on the vertices of the triangulation but entirely belong to a particular element of the mesh. This approximation is thus completely discontinuous between triangles. The nodal values of the non-conforming approximation are lying in the middle of the segments of the triangulation. This discrete solution is only continuous across triangle boundaries at mid-side nodes and discontinuous everywhere else around a triangle boundary.

We shall consider a partition $\mathcal{P}$ of Ω such that the restriction of s^h on $\mathcal{P}$ is continuous. In our presentation, there is only one subdomain for continuous approximations and N_E subdomains for discontinuous and non-conforming approximations. Discontinuous and non-conforming schemes are thus obtained by considering that each element of the triangulation is a subdomain Ω_i and that $s^h_{|\Omega_i}$ is continuous. It should be noticed that an equivalent approach would be to assume that there is only one subdomain $\Omega_1 = \Omega$ but that s^h may be discontinuous between triangles.

A finite element approximation to the exact solution of problem (1)-(2)-(3) is found by applying the variational formulation (6) to the discrete solution s^h. The nodal values are then found by using the Galerkin procedure which amounts to replace $\hat{s}$ by a basis function ϕ_i in (6)

for $1 \leq i \leq N$. For continuous, discontinuous and non-conforming finite element approximations, N is equal to N_V, $3N_E$ and N_S respectively. It should be noticed that the localized nature of discontinuous and non-conforming approximations permits to obtain a block diagonal global mass matrix with uncoupled blocks. Hence if the time stepping of the advection and diffusion terms is explicit, the resolution of the discrete equations does not require the use of a linear solver. This is not the case with continuous approximations.

To derive the finite volume scheme, we integrate equation (1) on each control volume by using Green's formula and replace s by a continuous approximation s^h. Hence we get N_V discrete equations which involve advective and diffusive flux budgets between control volumes. This can also be interpreted as considering a test function that is equal to one in the control volume and vanishes everywhere else and handling integrals by parts in a cautious way.

It should be noticed that the diffusion term of the non-conforming scheme can be simplified. Let us consider a node k shared by the elements Ω_i and Ω_j. The diffusion term and diffusive flux continuity constraint associated with node k can be written as:

$$\begin{aligned} A_k &= \int_{\Omega_i} K\boldsymbol{\nabla} s^h \cdot \boldsymbol{\nabla}\phi_k \ \mathrm{d}\Omega - \int_{\partial\Omega_i} K\boldsymbol{\nabla} s^h \cdot \mathbf{n}_i \phi_k \ \mathrm{d}\Gamma \\ &+ \int_{\partial\Omega_i} (K\boldsymbol{\nabla} s^h_{|\Omega_i} - K\boldsymbol{\nabla} s^h_{|\Omega_{nb_i}}) \cdot \mathbf{n}_i \ \frac{\phi_k}{2} \ \mathrm{d}\Gamma \\ &+ \int_{\Omega_j} K\boldsymbol{\nabla} s^h \cdot \boldsymbol{\nabla}\phi_k \ \mathrm{d}\Omega - \int_{\partial\Omega_j} K\boldsymbol{\nabla} s^h \cdot \mathbf{n}_j \phi_k \ \mathrm{d}\Gamma \\ &+ \int_{\partial\Omega_j} (K\boldsymbol{\nabla} s^h_{|\Omega_j} - K\boldsymbol{\nabla} s^h_{|\Omega_{nb_j}}) \cdot \mathbf{n}_j \ \frac{\phi_k}{2} \ \mathrm{d}\Gamma, \end{aligned}$$

where nb_i denotes the index of the elements neighboring Ω_i and sharing a common edge. Since the discrete solution is linear, it can be immediately observed that:

$$\int_{\Omega_{i,j}} K\boldsymbol{\nabla} s^h \cdot \boldsymbol{\nabla}\phi_k \ \mathrm{d}\Omega - \int_{\partial\Omega_{i,j}} K\boldsymbol{\nabla} s^h \cdot \mathbf{n}_{i,j} \phi_k \ \mathrm{d}\Gamma = 0.$$

Moreover, the gradient of s^h is constant and the integral of the diffusive flux on $\partial\Omega_i$ and $\partial\Omega_j$ is only non vanishing on the common interface Γ_l between Ω_i and Ω_j. This is due to the non-conforming shape function ϕ_k which is equal to 1 on Γ_l and linearly varies between -1 and 1 on the other edges. Hence, all boundary integrals reduce to an integral on the common edge Γ_l. The diffusion term may thus be rewritten as:

$$\begin{aligned} A_k &= \frac{1}{2}\int_{\Gamma_l} (K\boldsymbol{\nabla} s^h_{|\Omega_i} - K\boldsymbol{\nabla} s^h_{|\Omega_j}) \cdot \mathbf{n}_i \ \phi_k \ \mathrm{d}\Gamma \\ &\quad + \frac{1}{2}\int_{\Gamma_l} (K\boldsymbol{\nabla} s^h_{|\Omega_j} - K\boldsymbol{\nabla} s^h_{|\Omega_i}) \cdot \mathbf{n}_j \ \phi_k \ \mathrm{d}\Gamma, \\ &= \int_{\Gamma_l} K\boldsymbol{\nabla} s^h_{|\Omega_i} \cdot \mathbf{n}_i \ \phi_k \ \mathrm{d}\Gamma + \int_{\Gamma_l} K\boldsymbol{\nabla} s^h_{|\Omega_j} \cdot \mathbf{n}_j \ \phi_k \ \mathrm{d}\Gamma, \\ &= \int_{\Omega_i} K\boldsymbol{\nabla} s^h \cdot \boldsymbol{\nabla}\phi_k \ \mathrm{d}\Omega + \int_{\Omega_j} K\boldsymbol{\nabla} s^h \cdot \boldsymbol{\nabla}\phi_k \ \mathrm{d}\Omega. \end{aligned}$$

So, for non-conforming approximations, the discontinuous Galerkin formulation with weak constraints on the fluxes surprisingly appears to provide the same formulation as if we had simply omitted the boundary terms while performing the integral by parts. Hence, it seems that we commit a variational crime [20], but in fact, such a formulation is perfectly equivalent to the classical one. Moreover, as the integral of $[s^h]$ vanishes along each segment, we can drop the solution value continuity constraint. Hence, by construction, a weak continuity is automatically achieved for linear non-conforming shape functions. Those observations only hold for the linear non-conforming approximation which exhibits such a nice compromise between continuous and discontinuous interpolations.

VI. About local and global conservation

In this section we show that all the methods studied in the present paper are locally conservative. It is generally admitted that finite volume and discontinuous and non-conforming finite element schemes are locally conservative. This is due is to their formulation in term of flux budgets on an element basis. However continuous finite element schemes are usually said to be only globally conservative. Let us show that they are also conservative on individual elements.

We consider a generic time-dependent conservation law for a scalar quantity s:

$$\frac{\partial s}{\partial t} + \boldsymbol{\nabla} \cdot \boldsymbol{\sigma} = f, \tag{7}$$

where f is a source term and $\boldsymbol{\sigma}$ is a flux function. For the problem considered in the present paper:

$$\boldsymbol{\sigma} = \mathbf{u}s - K\boldsymbol{\nabla} s$$

and $f = 0$. We assume that the flux function is such that $\boldsymbol{\sigma} \cdot \mathbf{n} = 0$ on $\partial\Omega$.

Let us consider a subset Ω_e of Ω composed of one or several triangles E_i (Fig. 5) and let I_e be the ensemble of degrees of freedom associated with Ω_e. The discrete equations associated with Ω_e may be written as:

$$\int_{\Omega} \left(\phi_i \frac{\partial s^h}{\partial t} - \phi_i f - \boldsymbol{\nabla}\phi_i \cdot \boldsymbol{\sigma}\right) \mathrm{d}\Omega + \int_{\partial\Omega} \phi_i \boldsymbol{\sigma} \cdot \mathbf{n} \ \mathrm{d}\Gamma = 0 \quad \forall i \in I_e.$$

The integral on Ω may be decomposed into integrals on Ω_e and $\Omega \backslash \Omega_e$:

$$\begin{aligned} &\int_{\Omega_e} \left(\phi_i \frac{\partial s^h}{\partial t} - \phi_i f - \boldsymbol{\nabla}\phi_i \cdot \boldsymbol{\sigma}\right) \mathrm{d}\Omega \\ &+ \int_{\Omega\backslash\Omega_e} \left(\phi_i \frac{\partial s^h}{\partial t} - \phi_i f - \boldsymbol{\nabla}\phi_i \cdot \boldsymbol{\sigma}\right) \mathrm{d}\Omega \\ &+ \underbrace{\int_{\partial\Omega} \phi_i \boldsymbol{\sigma} \cdot \mathbf{n} \ \mathrm{d}\Gamma}_{=0} = 0 \quad \forall i \in I_e \end{aligned} \tag{8}$$

The first two terms of equation (8) are opposed and can be interpreted as the integral of the flux $\boldsymbol{\sigma} \cdot \mathbf{n}$ weighted by ϕ_i along the common interface [13]. The opposed signs refer to opposed normals respectively (the flux from Ω_e to $\Omega \backslash \Omega_e$ or the flux from $\Omega \backslash \Omega_e$ to Ω_e). In other words, if we consider

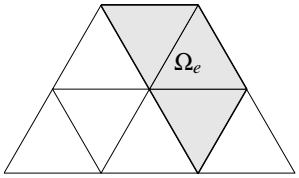

Fig. 5. Subset Ω_e (in gray) of the computational domain Ω.

a local problem restricted to Ω_e and wish to obtain a local solution exactly identical to the global solution, we shall impose a flux such that its weighed integral would provide exactly the same result as the second term of equation (8). It is well known that an accurate calculation of fluxes along interfaces of finite element meshes has to be performed in such a way (e.ge [14], [15], [16]). Hence equation (8) may be rewritten as:

$$\int_{\Omega_e} \left(\phi_i \frac{\partial s^h}{\partial t} - \phi_i f - \boldsymbol{\nabla}\phi_i \cdot \boldsymbol{\sigma}\right) \mathrm{d}\Omega + \int_{\overline{(\Omega \setminus \Omega_e)} \cap \bar{\Omega}_e} \phi_i \boldsymbol{\sigma} \cdot \mathbf{n} \, \mathrm{d}\Gamma = 0,$$

$\forall i \in I_e$. As $\boldsymbol{\sigma} \cdot \mathbf{n} = \mathbf{0}$ on $\partial\Omega$, we have:

$$\int_{\Omega_e} \left(\phi_i \frac{\partial s^h}{\partial t} - \phi_i f - \boldsymbol{\nabla}\phi_i \cdot \boldsymbol{\sigma}\right) \mathrm{d}\Omega + \int_{\partial\Omega_e} \phi_i \boldsymbol{\sigma} \cdot \mathbf{n} \, \mathrm{d}\Gamma = 0,$$

$\forall i \in I_e$. Summing all the discrete equations associated with the subset Ω_e leads to the integral form of the conservation law:

$$\frac{d}{dt} \int_{\Omega_e} s^h \, \mathrm{d}\Omega = \int_{\Omega_e} f \, \mathrm{d}\Omega - \int_{\partial\Omega_e} \boldsymbol{\sigma} \cdot \mathbf{n} \, \mathrm{d}\Gamma. \qquad (9)$$

This relation implies that the total amount of s^h in Ω_e may only change due to fluxes through the domain boundary and internal sources or sinks. The quantity s^h is thus conserved locally on Ω_e. The same argument may be used for finite volumes or discontinuous and non-conforming finite element methods. Hence all the methods examined in the present paper are elementwise conservative if fluxes are computed in an appropriate way.

VII. Dispersion analysis

In this section we present the dispersion relation of the discontinuous finite element scheme for an advection equation. A similar analysis is performed in [6] for a continuous stabilized finite element scheme. For the sake of simplicity, we shall consider the one-dimensional advection equation with a constant advecting velocity u:

$$\frac{\partial s}{\partial t} + \frac{\partial}{\partial x}(us) = 0.$$

This equation is solved on a 1D uniform grid with element size h. We seek solutions of the form $s(x,t) = \tilde{s} e^{-i\omega t + ikx}$, where k is the wave number in the $x-$direction, ω is the angular frequency and $\tilde{s}$ is a constant amplitude. This leads to the following dispersion relation for frequency:

$$\omega h/u = -2i - ie^{-ikh} \pm \sqrt{2 - 10e^{-ikh} - e^{-2ikh}}.$$

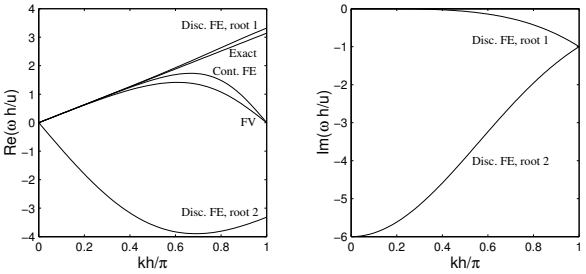

Fig. 6. Dispersion relations of the discontinuous finite element (Disc. FE), continuous finite element (Cont. FE) and finite volume (FV) schemes compared to the exact relation. The left and right panels represent the real and imaginary parts of the dispersion relation respectively.

The latter relation is compared with the dispersion relations of the finite volume and continuous finite element schemes in Fig. 6. Those relations respectively read:

$$\omega h/u = \frac{4\sin(kh)}{3+\cos(kh)},$$
$$\omega h/u = \frac{3\sin(kh)}{2+\cos(kh)}.$$

The real part of the dispersion relation shows that one of the two modes generated by the discontinuous scheme is non-physical and propagates in the wrong direction. However, as seen in the right panel, this mode is strongly damped since its imaginary part is negative for all wavelengths. As a result, it quickly disappears leaving only the physical mode.

On the other hand, the physical mode generated by the discontinuous scheme has good dispersive properties since $Re(\omega)$ is very close to the exact solution $\omega = uk$. Contrary to the finite volume and continuous finite element schemes, the dispersion relation of the discontinuous scheme is strictly monotonic and does not go to zero for $kh = \pi$. Hence, the speed at which energy propagates, given by the slope of the dispersion relation, is always positive and the scheme does not allow the existence of small-scale spurious oscillations. The continuous finite element and the finite volume schemes have similar dispersion curves even though the former exhibits slightly less dispersion than the latter.

The right panel shows the imaginary part of frequency. The frequencies of the exact, continuous finite element and finite volume solutions are strictly real and do not appear on the plot. The physical mode of the discontinuous scheme is only dissipative for high frequencies which is a desirable property. Hence the upwinding introduced in the scheme only has an effect on small scale features and leaves the main solution unchanged.

VIII. Numerical simulations and discussion

In this section, we perform some numerical experiments to assess the different numerical schemes introduced previously. A traditional test case to examine the behaviour

of transport schemes is the cone rotation test. This test involves the transport of a profile containing sharp discontinuities within a smooth velocity field. This situation is however rare in ocean modelling where the transport of a smooth tracer field in a localized, highly sheared current is more likely to happen. That's why we consider the more realistic test problem introduced in [17].

In their paper, the authors compare different finite difference advection schemes by considering the transport of a gaussian hill through the western boundary layer of a Stommel flow. A reference solution s^r can be built at each time step through the integration of the analytic velocity field to find the departure point corresponding to each arrival point on the grid. The same test problem is considered in [21] but for a rotated grid so that the western boundary current of the gyre is no longer aligned with one of the grid axes. This test is of course more severe for numerical schemes using a structured grid.

We consider a square $L \times L$ basin ($L = 10^6$ m) and a Stommel flow of which streamfunction is:

$$\Psi(x,y) = \frac{FL}{\pi\gamma\rho H}\cos(\frac{\pi y}{L})(pe^{xz_+} + qe^{xz_-} - 1),$$

where $0 \leq x, y \leq L$. The amplitude of the wind stress is $F = 0.1$ N/m^2, the frictional coefficient is $\gamma = 10^{-6}$ s^{-1}, the fluid layer density is $\rho = 1000$ kg/m^3 and the fluid layer depth is $H = 200$ m. The arguments and amplitudes of the exponential functions are

$$\begin{aligned} z_\pm &= -\frac{\alpha}{2} \pm \sqrt{\frac{\alpha^2}{4} + (\frac{\pi}{L})^2}, \\ p &= \frac{1 - e^{Lz_-}}{e^{Lz_+} - e^{Lz_-}}, \\ q &= 1 - p, \end{aligned}$$

where $\alpha = \beta/\gamma$ and β is the Coriolis factor first order derivative. The boundary layer width is of order of $\alpha^{-1} = 100$ km. The velocity $\mathbf{u} = (u, v)$ is found from the streamfunction:

$$u = \frac{\partial \Psi}{\partial y} \quad \text{and} \quad v = -\frac{\partial \Psi}{\partial x}.$$

The advection and diffusion terms are both discretized explicitly in time and the time step is set to 2500 s. The initial tracer field is given by the following expression:

$$s_0(x,y) = 10\exp(-\frac{((x - 2L/3)^2 + (y - L/3)^2)}{2(L/12.5)^2}).$$

Fig. 7 shows the stream function of the flow and the initial tracer field.

Errors on the discrete solution and its extrema are also computed for a more quantitative comparison. The L_2 error is defined as follows:

$$e_{L_2} = \frac{\left\| s^r - s^h \right\|_{L_2(\Omega)}}{\left\| s^r \right\|_{L_2(\Omega)}},$$

where $\|.\|_{L_2(\Omega)}$ is the L_2 norm on Ω. It is also useful to compare the numerical and reference solutions in terms

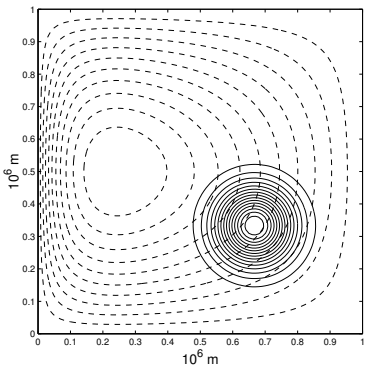

Fig. 7. Stream function of the flow (dashed line) and initial tracer distribution (solid line). The orientation of the flow is clockwise.

of minimum and maximum values. This permits for instance to estimate the importance of unphysical extrema generated by the numerical model. The absolute errors on minimum and maximum values read:

$$\begin{aligned} e_{min} &= \min_\Omega s^h - \min_\Omega s^r, \\ e_{max} &= \max_\Omega s^h - \max_\Omega s^r. \end{aligned}$$

One of the main advantage of unstructured grids is to allow a variable refinement. Hence it is in principle always possible to avoid under-resolved boundary currents. However that does not mean that in practice the resolution of all boundary layers will be optimal. For instance, commonly used viscosity values give western boundary widths ranging from 30 to 200 km [22]. An accurate representation of each boundary layer may thus be hard to achieve in a global circulation model, even with variable resolution. So, for the present experiment, we consider a grid with a slightly increased, but not optimal, resolution in the boundary layer.

A. Pure advection

We first study the transport of the tracer in a purely advective flow. The grid being totally unstructured, elements are not aligned with the boundary layer current and the experiment is thus comparable to that performed by [21]. Results for the different schemes are presented in Fig. 8 at different stages of the gaussian hill displacement. Error measures are given in Fig. 9.

Before the tracer field gets in the boundary layer, all schemes give similar results. Afterward, the L_2 error increases significantly for each scheme when the tracer goes through the boundary current. This increase is however more important for schemes using continuous approximations. When the tracer has left the boundary layer, the error committed by continuous schemes is more than twice larger than for discontinuous or non-conforming schemes. This is due to the lack of flexibility of continuous methods which prevents them from representing accurately solutions with steep gradients. As a result, they are prone to produce ripples that propagate in the domain and reflect on boundaries. An estimation of the ripples importance is given by

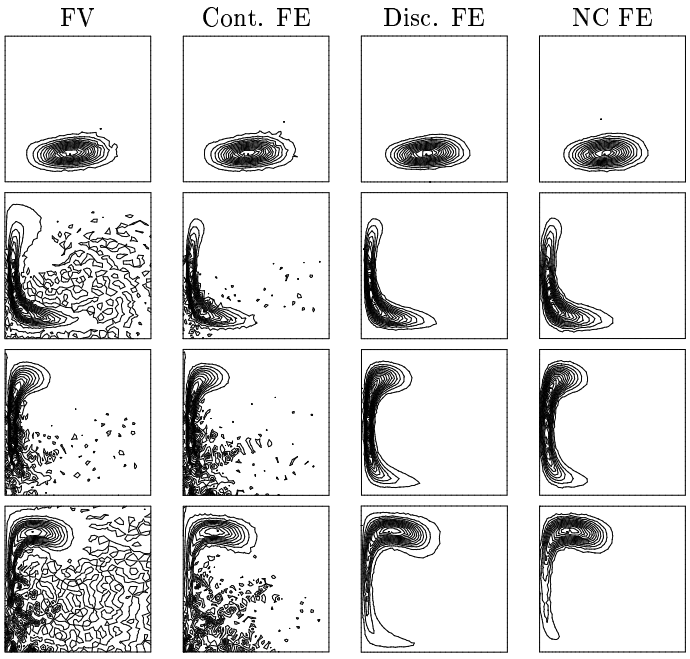

Fig. 8. Snapshots of the simulated tracer field after 2×10^6, 4×10^6, 5×10^6 and 6×10^6 seconds respectively for pure advection with the finite volume (FV), continuous finite element (Cont. FE), discontinuous finite element (Disc. FE) and non-conforming finite element (NC FE) schemes. There are 13 isolines.

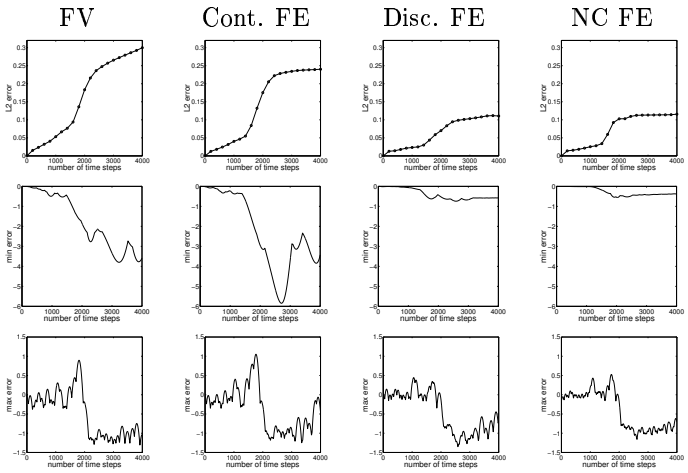

Fig. 9. L_2 (top), *min* (middle) and *max* (bottom) errors resulting from pure advection of the tracer profile.

the *min* error (Fig. 9). Hence for the finite element scheme, the largest downward ripple is nearly 60% as large as the initial peak value. There are yet stabilization procedures such as streamline diffusion or least-squares stabilization [23] that can be used to avoid unphysical extrema but they may have an important diffusive effect.

On the other hand discontinuous and non-conforming finite element schemes perform better. Their higher flexibility enables a more accurate representation of the solution in the boundary layer. The upwind-weighted formulation shows good shape preservation and much reduced rippling (Fig. 9). It must be pointed out that the upwind formulation does not have an important diffusive effect as the peak value of the tracer distribution does not decrease much (Fig. 9). Moreover the L_2 error stays constant when the tracer has left the boundary current which shows that upwinding has a negligible impact on the main solution.

It should be noticed that the advection schemes studied in the present paper are not monotonic by design. This is clearly seen on Fig. 9. Standard flux or solution limiters can be applied to the numerical solutions so as to render them monotonic. However, the use of such limiters will render the comparison of our schemes not so highlighting. Moreover the careful selection of suitable numerical parameters for such schemes needs further researches.

B. Advection and diffusion

Since ocean modelling is not a purely advective problem, it is interesting to see what happens if a physically realistic diffusivity is included. For the grid used in the present simulation, the average size of an element is of the order of 30 km. Hence, according to [24], a Laplacian diffusivity of 30 m^2/s should be used. The same numerical simulation as before is performed. Snapshots of the tracer distribution are presented in Fig. 10.

Results are now slightly better for the continuous finite element and finite volume schemes. Ripples have decreased but not disappeared and the tracer distribution is still very noisy. A much higher level of diffusion is needed to totally filter out oscillations. Discontinuous and non-conforming finite elements still give good results and the largest downward ripples are only 5% as large as the initial peak amplitude (Fig. 11). As diffusion increases, all schemes tend to give similar results.

Finally, it should be noticed that the comparison performed here could appear biased as the numerical schemes under consideration do not have the same number of degrees of freedom. Discontinuous and non-conforming approximations respectively have 6 and 3 times more degrees of freedom than continuous approximations. However discontinuous and non-conforming schemes do not require linear solvers and their computational cost thus is comparable to continuous schemes. In our implementation, continuous finite elements are the cheapest method but the other schemes are no more than 25 % more expensive.

IX. Conclusions

Discontinuous and non-conforming finite element schemes are well suited to advection dominated flows. The high flexibility inherent in those methods permit to represent accurately solutions with steep gradients. They naturally allow upwind-weighted formulations that greatly reduce unphysical oscillations usually generated by centered schemes. Such upwind formulations allow much smaller diffusivities that are in better accord with observations.

Continuous finite element and finite volume schemes have difficulties to represent advection dominated flows and are prone to generate ripples in regions with strong shear. A level of diffusion beyond physically realistic values is needed to avoid oscillations. Despite a smaller number of

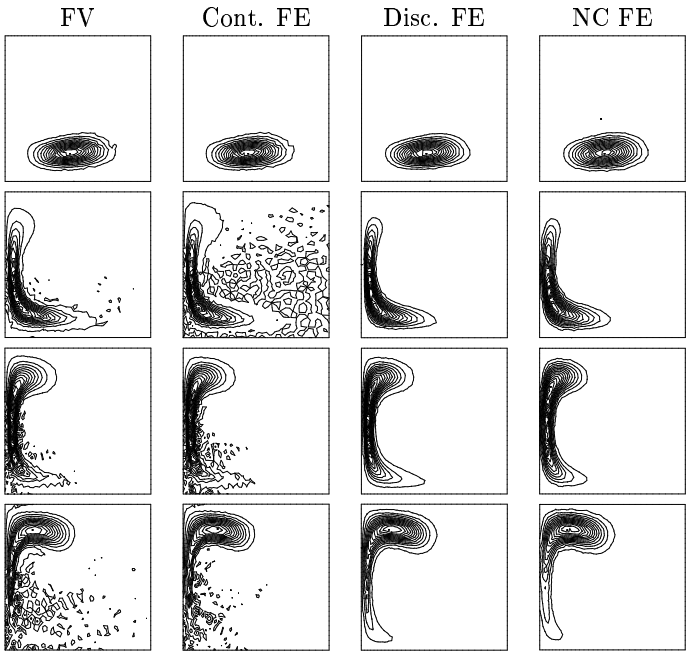

Fig. 10. Snapshots of the simulated tracer field after 2×10^6, 4×10^6, 5×10^6 and 6×10^6 seconds respectively for advection-diffusion ($K = 30$ m^2/s) with the finite volume, continuous finite element, discontinuous finite element and non-conforming finite element schemes. There are 13 isolines.

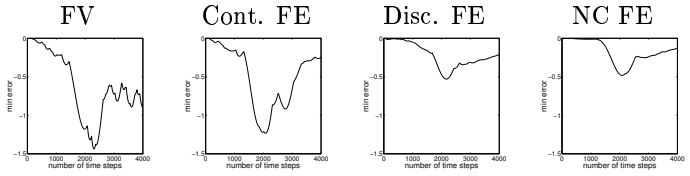

Fig. 11. *min* errors resulting from advection-diffusion of the tracer profile.

degrees of freedom, the computational cost of continuous methods is comparable to the one of discontinuous or non-conforming methods since the latter do not require linear solvers.

Discontinuous or non-conforming finite elements appear to be the most promising approximations to represent the evolution of scalar quantities in oceanic flows. Those schemes combine different properties such as flexibility, local conservation, upwinding and reasonable computational cost that would be particularly useful in ocean modelling.

Acknowledgments

Emmanuel Hanert and Eric Deleersnijder are Research fellow and Research associate, respectively, with the Belgian National Fund for Scientific Research (FNRS). The support of the Convention d'Actions de Recherche Concertées ARC 97/02-208 with the Communauté Française de Belgique is gratefully acknowledged.

References

[1] C. Le Provost, C. Bernier, and E. Blayo, "A comparison of two numerical methods for integrating a quasi-geostrophic multilayer model of ocean circulations : finite element and finite difference methods.," *Journal of Computational Physics*, vol. 110, pp. 341–359, 1994.

[2] P.G. Myers and A.J. Weaver, "A diagnostic barotropic finite-element ocean circulation model," *Journal of Atmospheric and Oceanic Technology*, vol. 12, pp. 511–526, 1995.

[3] D.R. Lynch, J.T.C. Ip, C.E. Naimie, and F.E. Werner, "Comprehensive coastal circulation model with application to the Gulf of Maine," *Continental Shelf Research*, vol. 16, pp. 875–906, 1996.

[4] D.Y. Le Roux, A. Staniforth, and C.A. Lin, "A semi-implicit semi-lagrangian finite-element shallow-water ocean model," *Monthly Weather Review*, vol. 128, pp. 1384–1401, 1999.

[5] D. Nechaev, J. Schröter, and M. Yaremchuk, "A diagnostic stabilized finite-element ocean circulation model," *Ocean Modelling*, vol. 5, pp. 37–63, 2003.

[6] S. Danilov, G. Kivman, and J. Schröter, "A finite element ocean model : principles and evaluation," *Ocean Modelling, in press*, 2003.

[7] R.J. Le Veque, *Finite Volume Methods for Hyperbolic Problems*, Cambridge University Press, 2002.

[8] P. Le Saint and P. Raviart, "On the finite element method for solving the neutron transport equation," *In C. de Boor, editor, Mathematical Aspects of Finite Elements in Partial Differential Equations, pages 89-145, New York,*, vol. Academic Press, 1974.

[9] B. Cockburn, G.E. Karniadakis, and C.W. Shu, *Discontinuous Galerkin Methods. Theory, Computation and Applications.*, Lecture notes in computational science and engineering. Springer, 2000.

[10] M. Crouzeix and P. Raviart, "Conforming and nonconforming finite-element methods for solving the stationary Stokes equations," *R.A.I.R.O. Anal. Numer.*, vol. 7, pp. 33–76, 1973.

[11] B.L. Hua and F. Thomasset, "A noise-free finite element scheme for the two-layer shallow water equations," *Tellus*, vol. 36A, pp. 157–165, 1984.

[12] D.Y. Le Roux, "Analysis of the $P_1^{NC}P_1$ finite-element pair in shallow-water ocean models," *Monthly Weather Review, submitted*, 2003.

[13] T.J.R. Hughes, G. Engel, L. Mazzei, and M.G. Larson, "The continuous galerkin method is locally conservative," *Journal of Computational Physics*, vol. 163, pp. 467–488, 2000.

[14] I. Babuska and A. Miller, "The post-processing approach in the finite element method. 1. calculation of displacements, stresses and other higher derivatives of the displacement," *International Journal for Numerical Methods in Fluids*, vol. 20, pp. 1085–1109, 1984.

[15] P.M. Gresho, R.L. Lee, R.L. Sani, M.K. Maslanik, and B.E. Eaton, "The consistent galerkin fem for computing derived boundary quantities in thermal and/or fluids problems," *International Journal for Numerical Methods in Fluids*, vol. 7, pp. 371–394, 1987.

[16] M Oshima, T.J.R. Hughes, and K. Jansen, "Consistent finite element calculation of boundary and internal fluxes," *International Journal of Computational Fluid Dynamics*, vol. 9, pp. 227–235, 1998.

[17] M.W. Hecht, W.R. Holland, and P.J. Rasch, "Upwind-weighted advection schemes for ocean tracer transport : An evaluation in a passive tracer context," *Journal of Geophysical Research*, vol. 100, pp. 20763–20778, 1995.

[18] E. Hanert, D.Y. Le Roux, V. Legat, and E. Deleersnijder, "Advection schemes for unstructured grid ocean modelling," *Ocean Modelling*, submitted.

[19] P. Houston, C. Schwab, and E. Suli, "Discontinuous $hp-$finite element methods for advection diffusion problems," Tech. Rep. NA-00/15, Oxford University, 2000.

[20] F. Thomasset, *Implementation of Finite Element Methods for Navier-Stokes Equations*, Springer Series in Computational Physics. Springer-Verlag, 1981.

[21] M.W. Hecht, B.A. Wingate, and P. Kassis, "A better, more discriminating test problem for ocean tracer transport," *Ocean modelling*, vol. 2, pp. 1–15, 2000.

[22] J. Yang, "On the importance of resolving the western boundary layer in wind-driven ocean general circulation models," *Ocean Modelling, in press*, 2003.

[23] T.J.R. Hughes, L.P. Franca, and G.M. Hubert, "A new finite element formulation for computational fluid dynamics: Viii. the Galerkin-least-squares method for advective-diffusive equations," *Computer methods in applied mechanics an engineering*, vol. 73, pp. 173–189, 1989.

[24] A. Okubo, "Oceanic diffusion diagrams," *Deep Sea Research*, vol. 18, pp. 789–802, 1971.